Comparative study of different erosion models in an Eulerian-Lagrangian frame using Open Source software

A. López[1*], M. T. Stickland[1] and W. M. Dempster[1]
[1]Mechanical and aerospace engineering, University of Strathclyde, Glasgow, UK
alejandro.lopez@strath.ac.uk

ABSTRACT

Erosion induced by particles striking on a surface is very common in many industrial processes and Computational Fluid Dynamics is one of the most widely used tools for erosion prediction. In this work the most commonly used erosion models are implemented and their review is carried out in OpenFOAM®, an open source CFD package. A comparison of the results yielded evident disparities in the location of the maximum erosion. Once an appropriate test rig is designed and the experimental work carried out, a more detailed assessment of the erosion models will be possible together with a study of the development of erosion with the deformation of the surface, relationship that none of the existing models accounts for.

1 INTRODUCTION

Throughout the years many authors have published a very large amount of papers and literature on erosion, having most of them developed their own equations for predicting erosive wear taking into account different approaches and factors that may influence erosion. An extensive literature review of more than 5000 articles was carried out by Meng and Ludema (1), having separated 28 erosion models out of the almost 2000 empirical models they encountered and concluding that each equation is the result of a very specific and individual approach. Prediction of erosion with the aid of CFD is based on the implementation of an erosion model suitable for the particular application and the attainment of the erosion rates and their location. The aim of this is usually the redesign of those parts of the equipment subjected to the highest erosion rates. In this article, some of the most commonly used erosion models are implemented in OpenFOAM, which is an Open Source CFD Package, and the resulting worn profile is compared against the experimental tests carried out by A.Gnanavelu et al.(2).

2   NOMENCLATURE

m_p = mass of the particle

u_p = velocity of the particle

x_p = position of the paticle

F_p = forces acting on the particle

F_D = Drag force

C_D = Drag coefficient

Re_P = Particle Reynolds number

ρ = Carrier phase density

d_p = Particle diameter

u = Carrier phase velocity

μ = Carrier phase dynamic viscosity

## 3   PARTICLE IMPINGEMENT CONDITIONS AND CFD MODEL

With the aid of Computational Fluid Dynamics (CFD), numerical solutions for the equations governing fluid flows can be successfully obtained in order to accurately predict the different outcomes of fluid-surface interactions. When dealing with the movement of a group of particles inside a fluid, there are basically two different ways to approach the problem. The first method is the Eulerian-Eulerian approach and it is suitable for large particle concentrations. In this kind of simulations, both particle-particle interactions and the influence of the particles on the fluid phase are important. On the other hand, in the Eulerian-Lagrangian approach, the Eulerian continuum equations are solved for the fluid phase, while Newton's equations for motion are solved for the particulate phase in order to determine the trajectories of the particles.
There are three different possibilities when constructing the equations that will define the motion of the particles inside the fluid phase:
- One way coupling: The influence that the particles exert on the fluid phase is neglected. This approach is suitable for low particle concentrations.
- Two way coupling: This methodology implies that the force the particles exert on the fluid is no longer neglected and a new term is incorporated into the fluid's equations to account for this.
- Four way coupling: In this case also particle-particle interactions are taken into account.
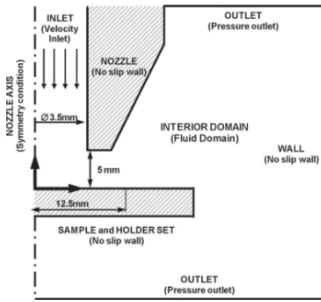
Figure 1: Configuration of the jet impingement test around the test probe (2).
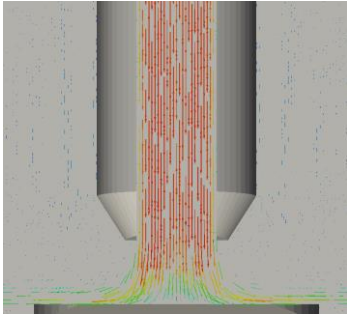
Figure 2: Velocity vectors around the test probe.

The trajectories of the particles are obtained once equations [1] and [2] have been solved:

$$m_p \frac{du_p}{dt} = \boldsymbol{F}_p \qquad [1]$$

$$\frac{dx_p}{dt} = \boldsymbol{u}_p \qquad [2]$$

In order to calculate the particle positions, first, the forces acting on the particle have to be defined. The force balance considered in this particular case on a spherical particle is shown in equation [3]:

$$F_p = m_p \frac{du_p}{dt} = \boldsymbol{F}_D \qquad [3]$$

The drag force on spherical particles is calculated in equation [4]:

$$F_D = m_P \frac{18\mu}{\rho_P d_P^2} \frac{C_D Re_P}{24} (\boldsymbol{u} - \boldsymbol{u}_P) \qquad [4]$$

And the drag coefficient (C_D) is obtained from equation [5]:

$$C_D = \begin{cases} \frac{24}{Re_P} \ if \ Re_P < 1 \\ \frac{24}{Re_P}(1 + 0.15 Re_P^{0.687}) if \ 1 \leq \ Re_P \leq 1000 \\ 0.44 \ if \ Re_P > 1000 \end{cases} \qquad [5]$$

while the particle Reynolds number is calculated with the aid of equation [6]:

$$Re_P = \frac{\rho|\boldsymbol{u} - \boldsymbol{u}_P|d_P}{\mu} \qquad [6]$$

Once the forces have been calculated, a first integration will yield the velocities and a further one will output the successive positions of the particles in the domain. Given that the concentration of particles inside the fluid in this case is very low (around 1%) and sufficient computational resources are available, the individual particles are tracked and every impact is monitored. Another typical approach would be to group several particles into a computational cloud. This construction is made because it is sometimes too expensive in computational terms to simulate all the real particles. In order to make a good approach to the real behaviour, some real case properties are defined. Selection of the correct approach includes the calculation of the particle mass loading (β) and the Stokes number (S_t) as in (3). The numbers obtained for this particular case were 0.003 and 26.29 respectively. These indicate the suitability of the one-way-coupled model for the disperse phase, given that the momentum transferred to the continuous phase is negligible, as it is also verified in the simulations. For this study, a CFD simulation of a Jet Impingement Test (JIT) has been chosen due to the range of impact conditions that it is able to reproduce as it is shown in Figure 2, where the fluid's velocity vectors are displayed. Prior to the introduction of the particles inside the domain, the steady-state is achieved for the fluid phase. The dispersed phase variables have been chosen in concordance with (2). The drag force is calculated for a uniform distribution of 250 μm diameter spherical sand particles impinging on a circular plate of 25 mm diameter. The variables which are going to be used in each of the different equations are gathered as the particles impact the surface and the damage produced at a cell by each impact is then calculated. The wear rate at each

cell will be the sum of the erosion produced by all the particle impacts. Transient simulations were carried out in OpenFOAM® in order to study the impingement conditions at each point on the surface. A study of the evolution of the angle of impingement with the distance from the centre of the jet was conducted. This was done by dividing the surface in 0.5 mm regions and calculating the mean of the angle of impingement for each region where impacts were detected. These values are shown in Figure 3, and the tendency of the angle of impingement to decrease with distance from the centre of the probe is clearly observed, which proves the suitability of JIT to simulate a wide range of impingement conditions.
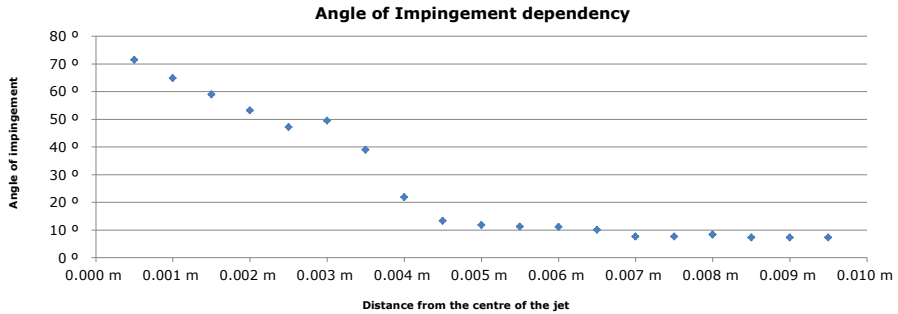
Angle of Impingement dependency

Figure 3: Angle of impingement dependency (degrees) in relation to distance from the centre of the jet (m).

4   Erosion modelling

Five different erosion models have been implemented and the experimental constants have been carefully adjusted for comparison between the wear scar yielded by each of the methods. However, provided that each equation takes into account different factors, the units used for erosion measurement are obviously altered. It is because of this that a qualitative analysis of the results is carried out along with an erosion profile comparison. The results are valid as long as the testing time is low enough so that no significant surface changes take place that are able to modify significantly the flow conditions around the wear scar, and thus modify the erosion pattern. The results show different wear scars for the exact same impingement conditions, i.e., number of impacts, location of these, angles of impingement and velocities at impingement.

3.1 Finnie erosion model (4)

The first set of equations [7] and [8], and also OpenFOAM®'s built in model, was developed by I. Finnie (4) and it yields the volume of material, Q removed by a single abrasive grain of mass, m, and velocity V:

$$Q = \frac{m V^2}{p \psi K} \left(\sin 2\alpha - \frac{6}{K} sin^2\alpha \right) \quad if \tan\alpha \leq \frac{K}{6} \qquad [7]$$

$$Q = \frac{m V^2}{p \psi K} \left(\frac{K cos^2\alpha}{6} \right) \quad if \tan\alpha \geq \frac{K}{6} \qquad [8]$$

Where p is the plastic flow stress of the material being eroded, α is the angle of impingement, ψ is a constant that represents the ratio of depth of contact to the depth of cut and K is the ratio of vertical to horizontal force components on the particle.

The main disadvantage of this equation lies in the discrepancy between experimental and theoretical results when the particles impact the surface at normal incidence. Finnie's equation yields accurate results for low angles of impingement but predicts no erosion for impacts normal to the surface.

Figures 4 and 5 show the erosion contours and profile respectively.
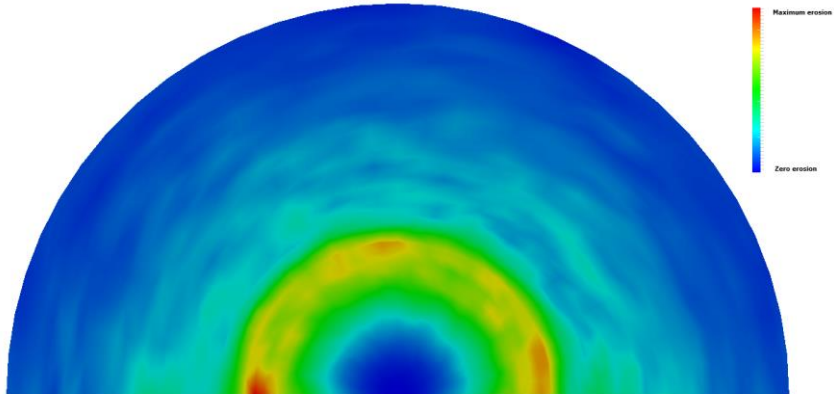
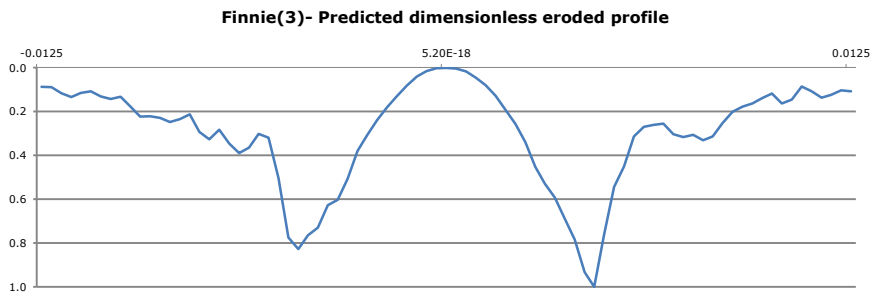Figure 4: I. Finnie (3) erosion contours obtained with OpenFOAM®.

Finnie(3)- Predicted dimensionless eroded profile

Figure 5: I. Finnie (3) eroded profile along a diameter of the circular test probe.

3.2 Grant and Tabakoff erosion model (5)

The empirical equation developed in (5) is based on the assumption that erosion is dependent on two different mechanisms; one acting at low angles of attack and the other at high angles of attack, as well as a combination of both when impacts take place at intermediate approach angles. This is shown in equation [9]:

$$\varepsilon = K_1 f(\beta_1)(V_{1T}^2 - V_{2T}^2) + f(V_{1N}) \tag{9}$$

Where:

ε = The erosion damage per unit mass of impacting particles

K_1 = Material contact

$f(\beta_1)$ = Empirical function of particle impact angle

V_{1T} = Tangential component of incoming particle velocity

V_{2T} = tangential component of rebounding particle velocity

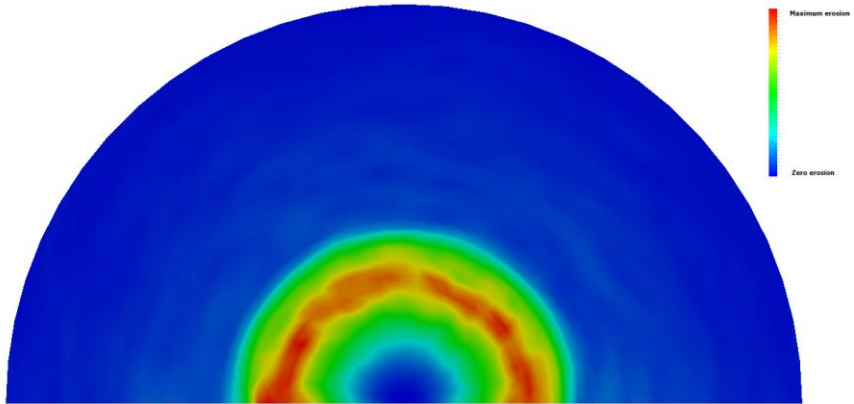$f(V_{1N})$ = Component of erosion due to the normal component of velocity

Figure 6: Grant and Tabakoff (5) erosion contours obtained with OpenFOAM®.

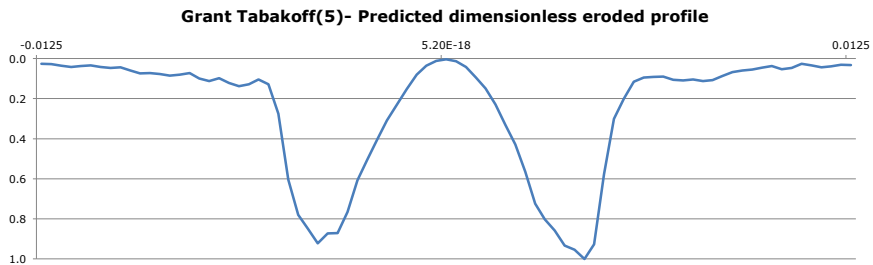**Grant Tabakoff(5)- Predicted dimensionless eroded profile**

Figure 7: Grant and Tabakoff (5) eroded profile along a diameter of the circular test probe.

Figures 6 and 7 show the results obtained with this erosion model. The location of maximum erosion differs from that found with the Finnie model. The model in this case is yielding no damage at the centre of the probe, though the size of this damage-free region is smaller than that of the previous erosion model, thus proving itself as a better approach.

3.3 Hashish erosion model (6)

M. Hashish modified Finnie's model for erosion by solid particle impingement in ductile materials taking into account particle shape and including no empirical constants. This model is suitable for shallow angles of impact in ductile materials (7). The equation, taken from (7), and used for the simulation is equation [10].

$$W = \frac{7}{\pi} \frac{M}{\rho_p} \left(\frac{V}{C_k}\right)^{2.5} \sin(2\alpha)\sqrt{\sin\alpha} \qquad [10]$$

Where,

M = Mass of the abrasive particles

ρ_p = Density of the particles

V = Velocity magnitude of the particles

α = Angle of impingement

C_k is a coefficient which can be obtained from equation [11].

$$C_k = \sqrt{\frac{3\sigma_f R_f^{\frac{3}{5}}}{\rho_p}} \qquad [11]$$

Where R_f is the roundness factor of the particulate phase.

Figures 8 and 9 show erosion results using Hashish's theoretical model. Discrepancies are, in this case, related to the relative magnitude of erosion taking place. The maximum erosion is in the same region as Grant and Tabakoff's model.
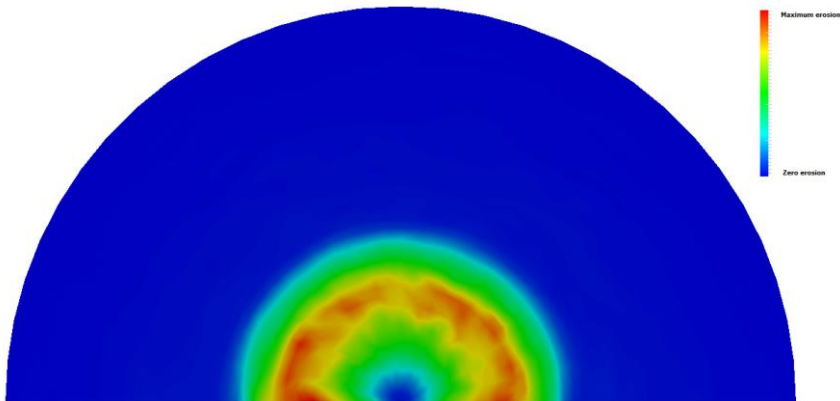

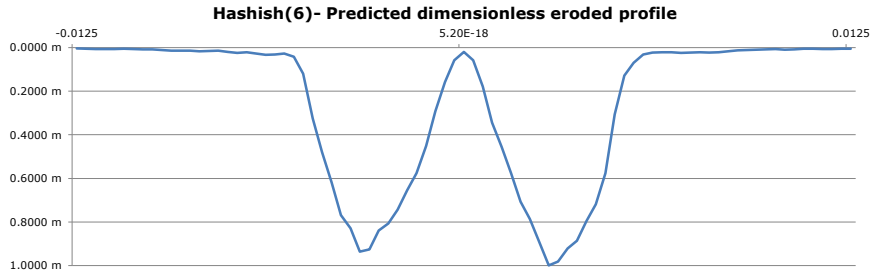**Figure 8: Hashish (6) erosion contours obtained with OpenFOAM®.**

Figure 9: Hashish (6) eroded profile along a diameter of the circular test probe.

3.4 Nandakumar et al. erosion model (8)

Taking as a starting point Bitter's(9,10) and Finnie's (11) work , and thus dividing the erosion into cutting and deformation wear, K. Nandakumar et al (8), developed an erosion model that predicts the volume eroded by successive impacts of particles on a surface.
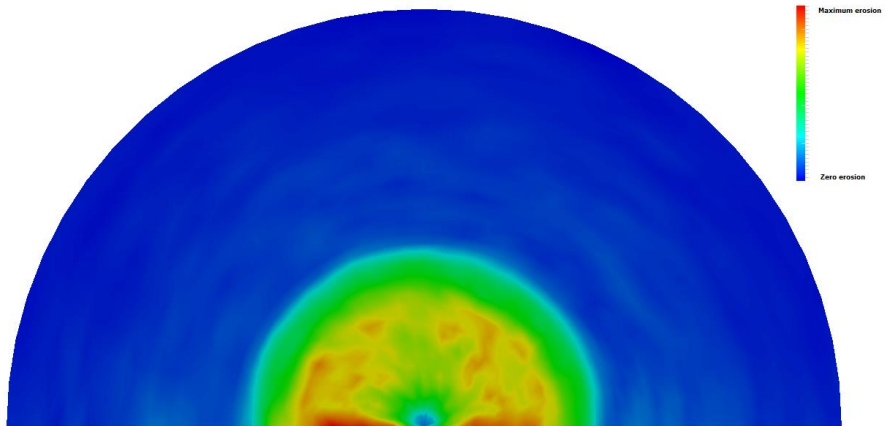

Figure 10: Nandakumar et al (8) erosion contours obtained with OpenFOAM®.

The equation developed and used in the simulations is equation [12]:

$$\Delta Q = Cm\rho_p^{0.15}(V_0 sin\theta)^{2.3} + Dm^{1.1875}d_p^{-0.0625}V_0^{2.375}(cos\theta)^2(sin\theta)^{0.375} \hspace{2cm} [12]$$

Where C and D are empirical constants, m is the mass of the particle, ρ_p is the density of the particle, θ is the angle of impact, V_0 is the impact velocity and d_p is the diameter of the particle.
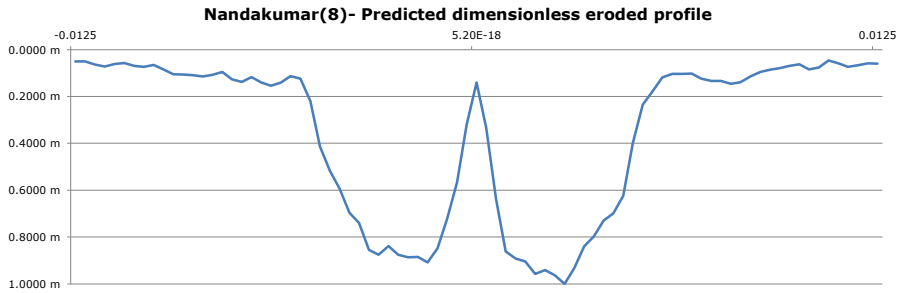
Nandakumar(8)- Predicted dimensionless eroded profile

Figure 11: Nandakumar et al (8) eroded profile along a diameter of the circular test probe.

Prediction with Nandakumar's model yields non-zero magnitude of erosion for the central part of the probe. Figures 10 and 11 show Nandakumar's model predictions.

3.5 Hutchings erosion model (12)

This last model was developed by I. M. Hutchings in 1981 and it is based on the assumption that a fragment of material will be removed when the maximum plastic strain within that fragment reaches a critical value denoted by ϵ_c, which has to be determined experimentally together with α; the fraction of the volume of indentation plastically deformed. Erosion in this case is given by equation [13]:

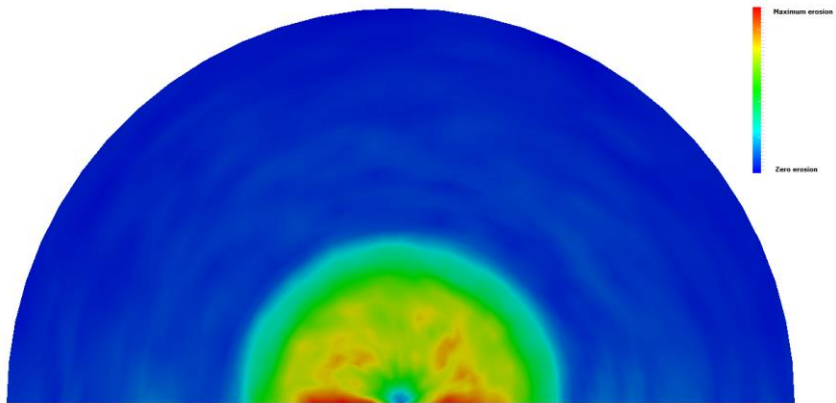$$E = 0.033 \frac{\alpha \rho \sigma^{\frac{1}{2}} v^3}{\epsilon_c^2 P^{\frac{3}{2}}}$$

[13]

Figure 12: Hutchings (12) erosion contours obtained with OpenFOAM®.

Where v is the velocity of the particles at impingement and P, ρ and σ are the dynamic hardness, the density and the plastic flow stress of the material being eroded respectively.

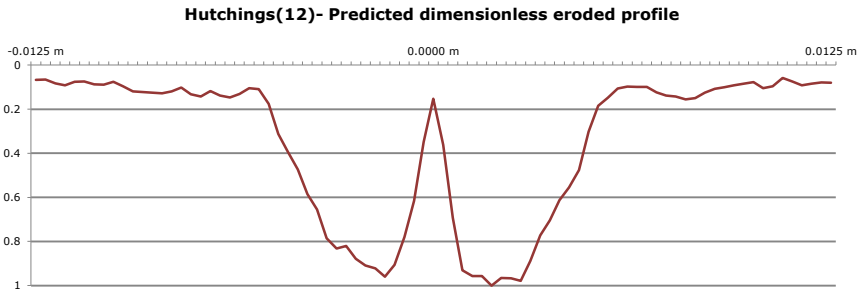**Hutchings(12)- Predicted dimensionless eroded profile**

Figure 13: Hutchings (12) eroded profile along a diameter of the circular test probe.

Models by Hutchings and Nandakumar yield very similar results in this particular case, differing only in the magnitude and predicting maximum erosion taking place on the same region of the test probe.

5   Results comparison

With a total of more than 700,000 particle impacts registered, Figure 14 shows the differences between normalised wear profiles yielded by each of the models. All of them show the existence of a stagnation point at the centre of the probe, which is in accordance with the experimental results shown in Figure 15 (2).
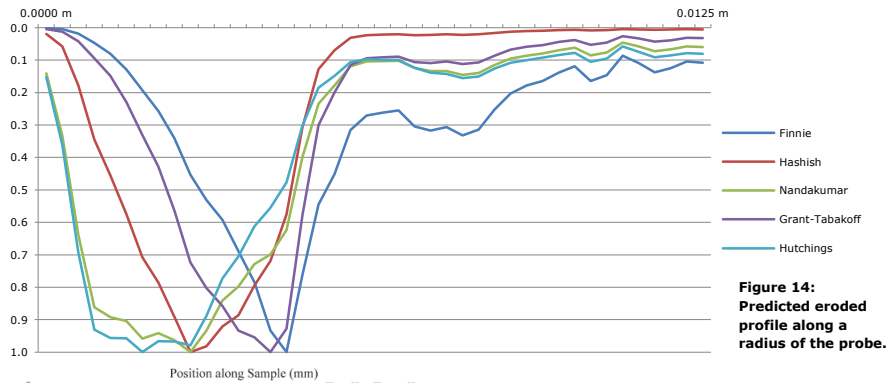

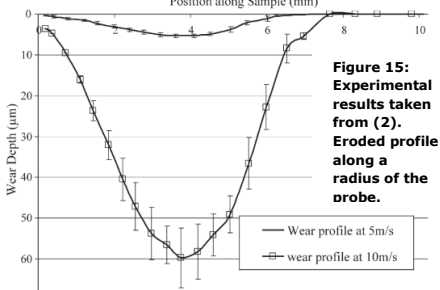Figure 14: Predicted eroded profile along a radius of the probe.

Figure 15: Experimental results taken from (2). Eroded profile along a radius of the probe.

As previously stated, Finnie's model shows no erosion on the central part of the probe, while Hashish and Grant and Tabakoff's models show very little damage at this location. It is only Hutchings and Nandakumar's models that are able to predict erosion on the central part of the probe, that is to

be expected in the JIT for ductile materials.

In order to obtain a quantitative comparison of the results, it seems adequate to scale the normalised profile to the order of magnitude of the experiments and see how the predicted wear scar matches the latter. This comparison is presented in Figure 16.
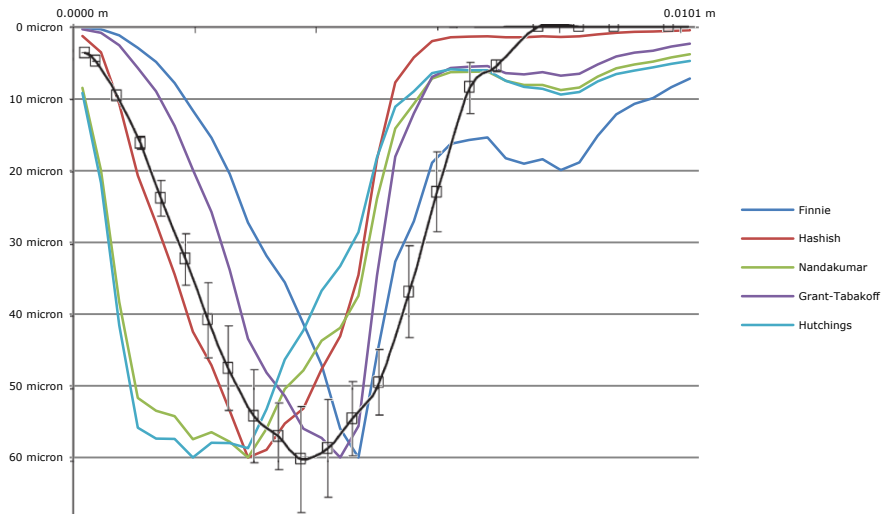
Figure 16: Quantitative comparison of the experimental wear profile taken from (2) with the profiles yielded by the different erosion models.

6 Conclusions

It is common to most wear models that they are only suitable for a process where similar impingement conditions take place and to be in need of obtaining the model constants through experimentation in case a different material is used. For this reason, Hashish's model for erosion would be a reasonable approach when experimentation is not feasible. The comparison with experimental results in figure 16 proves that despite having no experimentation, Hashish's formula is fairly accurate at capturing the position of the maximum erosion as well as the overall shape of the wear profile. On the other hand, either if the necessary data or experiments have been already carried out and are available, or if it is possible to obtain those empirical constants, Hutchings or Nandakumar's models would definitely reproduce the wear scar more accurately. However, as the surface profile continues to change with time, none of these methods would be able to do any more than show an initial location of erosion inside the geometry. For the attainment of accurate wear profiles after longer periods of time, a more complex model should be developed that accounts for surface deformation and its effect on the fluid flow as well as on the velocity and angle of impingement of the solid particles.

7   Acknowledgement

8   References

(1)   H.C. Meng, K.C. Ludema: Wear models and predictive equations: their form and content, Wear, Vol. 181-183 (1995), pp. 443-457.

(2)   A.Gnanavelu et al.: An integrated methodology for predicting material wear rates due to erosion, *Wear*, Vol. 267 (2009), pp. 1935–1944.

(3)   G.J. Brown: Erosion prediction in slurry pipeline tee-junctions. *Applied mathematical modeling*, Vol. 26 (2002), pp. 155-170.

(4)   I. Finnie: Erosion of surfaces by solid particles, *Wear*, Vol. 3 (1960), pp. 87–103.

(5)   Grant G. and Tabakoff W.: An experimental investigation of the erosion characteristics of 2024 aluminum alloy, *Department of Aerospace Engineering Tech. Rep.* (1973) 73-77, University of Cincinnati.

(6)   Hashish M. Modified model for erosion. *Proceedings of the 7th International Conference on Erosion by liquid and solid impact*, 1987, Cambridge, UK, pp. 461–480

(7)   M.S. ElTobgy et al.: Finite element modeling of erosive wear. *International Journal of Machine Tools and Manufacture*, Vol. 45 (2005), pp. 1337-1346.

(8)   K. Nandakumar et al.: A comprehensive phenomenological model for erosion of materials in jet flow, *Powder Technology*, Vol. 187 (2008), pp. 273-279.

(9)   J. G. A. Bitter: A study of erosion phenomena Part I, *Wear*, Vol. 6 (1963), pp. 5-21.

(10) J. G. A. Bitter: A study of erosion phenomena Part II, *Wear*, Vol. 6 (1963), pp. 169-190.

(11) I. Finnie: Some observations on the erosion of ductile metals, *Wear*, Vol. 19 (1972), pp. 81–90.

(12) I. M. Hutchings: A model for the erosion of metals by spherical particles at normal incidence, *Wear*, Vol. 70 (1981), pp. 269-281.